ISSN 2176-5480

22nd International Congress of Mechanical Engineering (COBEM 2013)
November 3-7, 2013, Ribeirão Preto, SP, Brazil

EFFICIENT NUMERICAL TOOLS TO INVESTIGATE HYPERBOLIC DYNAMICAL STRUCTURES IN A SPATIAL THREE-BODY SYSTEM

Priscilla A. Sousa-Silva
Universitat de Barcelona - Spain
priandss@maia.ub.es

Maisa de Oliveira Terra
ITA - Departamento de Matématica - São José dos Campos, Brazil
maisa@ita.br

Abstract. *We review and implement efficient methods to investigate hyperbolic dynamical structures in the Spatial Circular Restricted Three-Body Problem (SCR3BP). We aim to obtain invariant objects related to the practical stability domains around the triangular equilibrium points of the SCR3BP. These domains are regions in the phase space where trajectories remain confined for very long time spans. The Trojan asteroids that follow the orbit of Jupiter around the Sun are a popular example of the existence of such domains in natural systems. In this work, we employ suitable algorithms to compute hyperbolic invariant objects in the center manifold of L_3 of the Sun-Jupiter system, namely hyperbolic periodic orbits and two-dimensional tori with their stable and unstable invariant manifolds. Correspondence checks between these numerically constructed structures and approximated solutions obtained from the analysis of capture-escape transitions can establish whether these objects play a role in the determination of the effective stability boundaries that offer a preliminary model for the motion of the Trojans.*

Keywords: *efficient numerical algorithms, hyperbolic dynamical structures, astrodynamics, high-dimensional systems, capture-escape transition*

1. INTRODUCTION

It is known that the invariant manifolds of a dynamical systems organize the behavior of general solutions in the phase space. Such is their importance that hyperbolic invariant solutions are often regarded as the skeleton of a dynamical system. As a matter of fact, transversal intersections of stable and unstable invariant manifolds lead to homoclinic and heteroclinic phenomena responsible for unpredictability of solutions which is a signature of chaotic behavior (Wiggins (2003)). Thus, the investigation of such objects is of fundamental importance to understand and control the evolution of any system with practical applicability.

Let us consider the Spatial Circular Restricted Three-Body Problem (SCR3BP). This particular system has a wide variety of applications in Astronautics and Astrodynamics. For instance, it has been applied to design trajectories for modern space mission projects (e.g. SOHO, Genesis, ISEE-3, etc.) with requirements that cannot be met by the Keplerian decomposition of the Solar System. The theoretical framework for the construction of such trajectories has been widely explored by Gómez *et al.* (2001c,d,a,b); Koon *et al.* (2006); Marsden and Ross (2005). Also, the SCR3BP gives a suitable model for the motion of the Trojan asteroids in the Sun-Jupiter system (Robutel and Souchay (2010); MPC (2013)), for the dynamics of the sharp-edged rings of Uranus which are determined by the gravitational action of the shepherd moons Cordelia and Ophelia (Benet (2001)), and for the motion of some comets and asteroids known as Near Earth Objects (NEO) (NASA (2013)).

The hyperbolic invariant manifolds of the SCR3BP are the backbone that allow the diverse applications mentioned above. In particular, these structures are related to capture-escape behavior and to the determination of domains of effective or practical stability. These domains are regions in the phase space where the particles remain confined for long periods of time due to the presence of codimension-1 hyperbolic invariant manifolds that act as effective barriers between captured and escaping trajectories (Simó (1998)).

We recall (see Szebehely (1967) for more details) that the SCR3BP describes the motion of a particle of negligible mass moving under the gravitational influence of two bodies called the primaries and denoted by P_1 and P_2. The primaries have masses m_1 and m_2, respectively, and describe circular coplanar orbits around the barycenter of this two-body system, so that they are fixed in the synodic reference frame (which rotates with respect to an inertial frame). In this frame and using dimensionless variables, the equations of motion of the particle are

$$\ddot{x} - 2\dot{y} = \Omega_x,\ \ddot{y} + 2\dot{x} = \Omega_y,\ \ddot{z} = \Omega_z, \tag{1}$$

with the effective potential given by

$$\Omega(x, y, z) = \frac{1}{2}(x^2 + y^2) + \frac{1-\mu}{r_1} + \frac{\mu}{r_2} + \frac{\mu(1-\mu)}{2}, \tag{2}$$

ISSN 2176-5480

where the mass parameter $\mu = m_2/(m_1+m_2)$, $m_1 > m_2$, is the only parameter of the model, and $r_1 = \sqrt{(x-\mu)^2+y^2+z^2}$ and $r_2 = \sqrt{(x+1-\mu)^2+y^2+z^2}$ denote the distance from the particle to P_1 and P_2, located at $(\mu, 0, 0)$ and $(\mu - 1, 0, 0)$, respectively.

The system has an energy-like integral and its Hamiltonian reads

$$H(x,y,z,p_x,p_y,p_z) = \frac{1}{2}(p_x^2+p_y^2+p_z^2) + yp_x - xp_y - \frac{1-\mu}{r_1} - \frac{\mu}{r_2}, \tag{3}$$

where $p_x = \dot{x} - y$, $p_y = \dot{y} + x$, and $p_z = \dot{z}$ are the conjugate momenta of x, y, and z. Also, it presents two symmetries: the time reversal symmetry across the plane $y = 0$, $S_1 = \{(x, y, z, \dot{x}, \dot{y}, \dot{z}, t) \to (x, -y, z, -\dot{x}, \dot{y}, -\dot{z}, -t)\}$, and the mirror symmetry across the plane $z = 0$, $S_2 = \{(x, y, z, \dot{x}, \dot{y}, \dot{z}, t) \to (x, y, -z, \dot{x}, \dot{y}, -\dot{z}, t)\}$.

Five equilibrium points are found for the system of equations. Three of them, L_1, L_2, and L_3, are located on the x-axis. The other two, L_4 and L_5, are located in position space at $(\mu - 1/2, \mp 3^{1/2}, 0)$, at the vertices of equilateral triangles formed with the primaries. As it is well known, the triangular equilibrium points of the SCR3BP are linearly stable for $\mu \in (0, \mu_1)$, where $\mu_1 = (9 - \sqrt{69})/18$ is the Routh critical value, and Markeev (1972) showed that L_4 and L_5 are non-linearly stable in this interval, except also for $\mu_2 = (45 - \sqrt{1833})/90$, $\mu_3 = (15 - \sqrt{213})/30$ and a set of initial conditions of small Lebesgue measure for fixed μ.

The SCR3BP is an autonomous non-integrable Hamiltonian system with three degrees of freedom (i.e., six-dimensional phase space), so some amount of Arnold diffusion is to be expected in the five-dimensional energy shell. However, Giorgilli *et al.* (1989) found a bound to the rate of diffusion and obtained Nekhorosev-like estimates that predict local stability of trajectories in a vicinity of L_4 and L_5 up to finite but long time. Also, there is numerical evidence of the existence of domains (that can be quite large depending on the mass parameter) where the trajectories inherit the stable behavior of the equilibrium points during long spans of time (Simó (1998, 2006)).

Recent results show that several codimension-1 manifolds play a role in the definition of the sharp boundaries of such domains. Particularly, for $\mu = 0.0002$ two different situations are described by Simó *et al.* (2012, 2013a,b). In the first scenario the quasi-confinement of trajectories is related to the hyperbolic manifolds of the center manifold of the collinear libration point L_3 which is of centre-centre-saddle type. In the second scenario, confinement is related to the hyperbolic manifolds of the center manifold associated to a family of symmetric periodic orbits that bifurcate from the vertical periodic orbit near the center manifold of $L_{4,5}$. Inside each four-dimensional center manifold there are periodic and quasi-periodic solutions, with specific characteristics (such as period, rotation number, stability properties, etc.), and also small chaotic zones. Preliminary analyses of capture-escape transitions by Simó (1998) indicated especially significant quasi-periodic solutions inside these center manifolds. More recently, through a systematic investigation, Simó *et al.* (2013a) established which are the families of two-dimensional hyperbolic tori are located at the boundaries of effective stability domains. In fact, orbits outside but near the stability region depart from its vicinity guided by the three-dimensional unstable manifolds of these tori.

In order to understand the transport mechanisms related to capture-escape processes, one needs to be able to identify, compute and characterize the objects that play a role in the determination of the stability domains. Usually, formal calculations give a good representation of these solutions only in a domain of small to moderate size, so numerical methods have to be used to globalize these structures. Among other things, one needs numerical tools to: (i) detect the quasi-stable regions, (ii) identify different invariant structures at the stability boundaries, such as hyperbolic periodic orbits and two-dimensional tori, and (iii) compute these invariant objects and their stable and unstable manifolds.

It is valuable to note that we are interested in global five-dimensional unstable structures in a six-dimensional phase space (or four-dimensional unstable structures in the five-dimensional energy shell), therefore, the computation and the characterization of such objects require specific analytical and numerical techniques that take into account both their unstable character and high-dimension. Also, the substantial computing time needed to obtain global stability domains and families of two-dimensional tori with their hyperbolic manifolds is a concrete challenge that has to be overcome through the implementation of efficient algorithms that often need to be modified to deal with specificities found along the stability boundaries.

In what follows we review methods to numerically compute invariant objects at the boundaries of practical stability domains around the triangular equilibria of the SCR3BP. Then, we apply these techniques to the concrete case of the mass parameter corresponding to the Sun-Jupiter system and obtain several unstable periodic orbits and two-dimensional tori with their hyperbolic invariant manifolds.

2. THEORETICAL BACKGROUND

We will highlight the theoretical background we employ to compute unstable periodic orbits, hyperbolic two-dimensional tori and their stable and unstable invariant manifolds. Some general aspects of the methods described here can be found in Simó (1990). Specific references are given along the text when necessary.

The dynamical system given by Eq. (1) can be rewritten as a system of six first-order differential equations given, generically, by $\dot{\mathbf{z}} = f(\mathbf{z})$, $\mathbf{z} \in \mathbb{R}^6$, with $\mathbf{z}^T = (z_1, z_2, z_3, z_4, z_5, z_6)$. For a given initial condition $\mathbf{z}^0$, the solution of the

ISSN 2176-5480

system, or the flow, is the curve $\phi_t(\mathbf{z}^0)$. Due to the conservation of energy, the motion in the six-dimensional phase space is effectively restricted to five dimensions. Another dimension is reduced by working with adequate Poincaré sections. That is, let Σ be a section transversal to the flow, we define the four-dimensional Poincaré map $\mathcal{P} : \mathbb{R}^4 \to \mathbb{R}^4$ associated to Σ and work within that map.

2.1 Computing periodic orbits

Considering the Poincaré map $\mathcal{P}$ and the conservation of energy, the search for a periodic solution of the system of equations given by Eq. (1) is reduced to finding a point $\mathbf{w} \in \mathbb{R}^4$ such that $F(\mathbf{w}) = \mathcal{P}(\mathbf{w}) - \mathbf{w} = 0$. To this end, we use the Newton method: let

$$F(\mathbf{w}+\delta) = F(\mathbf{w}) + \frac{\partial F}{\partial \mathbf{w}}\delta + \mathcal{O}(\delta^2), \quad \text{with} \quad \frac{\partial F}{\partial \mathbf{w}} = D\mathcal{P} - \mathbf{I}, \tag{4}$$

where $D\mathcal{P} = \partial P/\partial \mathbf{w}$ is the differential of the Poincaré map. We want δ such that $F(\mathbf{w}+\delta) = 0$, that is, we solve the linear system

$$(D\mathcal{P} - \mathbf{I})\delta = \mathbf{w} - \mathcal{P}(\mathbf{w}) \tag{5}$$

repeatedly until the solution converges up to a desired accuracy.

In order to compute $D\mathcal{P}$ we need to obtain the Jacobian of the flow corrected at Σ: let

$$f(\mathbf{z}^0 + \Delta\mathbf{z}) - f(\mathbf{z}^0) = \frac{\partial \phi_t(\mathbf{z}^0)}{\partial \mathbf{z}}\Delta\mathbf{z} + \mathcal{O}(\varepsilon^2) + \frac{\partial f}{\partial t}\Delta t, \tag{6}$$

where $\dfrac{\partial \phi_t(\mathbf{z}^0)}{\partial \mathbf{z}}$ is the variational of the field, $\dfrac{\partial f}{\partial t}$ is the vector field computed when the trajectory returns to Σ and $\Delta\mathbf{z}$ are the deviations of the initial condition. The left side of Eq. (6) is denoted by $d\mathbf{z}$ and corresponds to the correction of the solution.

As a concrete example, let Σ be defined by $z_3 = 0$. Then, in matrix form, Eq. (6) is

$$d\mathbf{z} = \mathbf{A}\Delta\mathbf{z} + \mathbf{f}\Delta t, \tag{7}$$

where $\mathbf{A}$ is a 6×6 matrix with elements denoted by a_{ij}, $i, j = 1, .., 6$. Given that $\Delta z_3 = dz_3 = 0$ in Σ, the third component of Eq. (7) gives $\Delta t = -\{a_{31}\Delta z_1 + a_{32}\Delta z_2 + a_{34}\Delta z_4 + a_{35}\Delta z_5 + a_{36}\Delta z_6\}/f_3$, which is the correction in time needed so that the corrected solution lands on the Poincaré section after one iteration of the Newton method. Using the conservation of the energy ($H(\mathbf{z}^0 + \Delta\mathbf{z}) = H(\mathbf{z}^0)$) we write Δz_6 as a function of the other variations and get

$$\Delta t = -\frac{1}{f_3}\{(a_{31} + a_{36}\beta_1)\Delta z_1 + (a_{32} + a_{36}\beta_2)\Delta z_2 + (a_{34} + a_{36}\beta_4)\Delta z_4 + (a_{35} + a_{36}\beta_5)\Delta z_5\}, \tag{8}$$

with $\beta_1 = (f_4^0 - 2f_2^0)/f_3^0$, $\beta_2 = (f_5^0 + 2f_1^0)/f_3^0$, $\beta_4 = -f_1^0/f_3^0$ and $\beta_5 = -f_2^0/f_3^0$, where f^0 denotes the vector field at the initial condition. Finally, we get $D\mathcal{P}$ by replacing Eq. (8) in the other components of vector Eq. (7) so that

$$\begin{pmatrix} dz_1 \\ dz_2 \\ dz_4 \\ dz_5 \end{pmatrix} = \begin{pmatrix} p_{11} & p_{12} & p_{14} & p_{15} \\ p_{21} & p_{22} & p_{24} & p_{25} \\ p_{41} & p_{42} & p_{44} & p_{45} \\ p_{51} & p_{52} & p_{54} & p_{55} \end{pmatrix} \begin{pmatrix} \Delta z_1 \\ \Delta z_2 \\ \Delta z_4 \\ \Delta z_5 \end{pmatrix}, \quad \text{with} \tag{9}$$

$$p_{ij} = a_{ij} + a_{i6}\beta_j - \frac{f_i}{f_3}(a_{3j} + a_{36}\beta_j), \quad \text{for} \quad i, j = 1, 2, 4, 5. \tag{10}$$

2.2 Computing two-dimensional invariant tori

Let $\mathbb{T}^1$ denotes a one-dimensional torus with length equal to 2π. Let us look for invariant curves $\mathbf{y} : \mathbb{T}^1 \to \mathbb{R}^4$ of the Poincaré map $\mathcal{P}$. Following Castellà and Jorba (2000), we obtain these curves using a method based on the computation of the Fourier Coefficients of a parametrization of the curves.

Let ω be the rotation number of the curve. Then, the invariance condition is given by

$$\mathcal{P}(\mathbf{y}(\theta)) = \mathbf{y}(\theta + \omega), \ \ \forall \ \theta \in \mathbb{T}^1. \tag{11}$$

We assume that ω is known and write $\mathbf{y}(\theta)$ as a real Fourier series,

$$\mathbf{y}(\theta) = a_0 + \sum_{k>0} a_k \cos(k\theta) + b_k \sin(k\theta), \quad k \in \mathbb{N}, \quad \text{with} \quad a_0, a_k, b_k \in \mathbb{R}^4, \tag{12}$$

ISSN 2176-5480

which is truncated to order N so that an approximation of $2N+1$ coefficients (a_0, a_k and b_k with $0 < k \leqslant N$) can be determined.

We select $2N+1$ points along $\mathbb{T}^1$ by

$$\theta_j = \frac{2\pi j}{2N+1},\ 0 \leqslant j \leqslant 2N \tag{13}$$

and impose the invariance condition upon this points. This gives

$$\mathcal{P}(\mathbf{y}(\theta_j)) - \mathbf{y}(\theta_j + \omega) = 0,\ 0 \leqslant j \leqslant 2N, \tag{14}$$

which is a system of $2N+1$ equations. Then the Newton method is used to correct the $2N+1$ unknown Fourier coefficients.

Let $F : \mathbb{R}^{2N+1} \to \mathbb{R}^{2N+1}$ be a function that associates a set of Fourier coefficients $(a_0, a_1, b_1, a_2, b_2, \ldots, a_N, b_N)$ to the $2N+1$ values at the left side of Eq. (14). Each iteration of the Newton method requires the numerical evaluation of F in the Poincaré section Σ associated to the map $\mathcal{P}$, as well as the evaluation of the differential DF of F, where DF is a matrix composed of $(2N+1) \times (2N+1)$ blocks of matrices 4×4 with elements $(DF)_{jk}$ given by:

$$\begin{aligned} \frac{\partial F}{\partial a_k} &= D\mathcal{P}(\mathbf{y}(\theta_j))\mathbf{I}_4 \cos(k\theta_j) - \mathbf{I}_4(\cos(k\theta_j + k\omega)) \\ \frac{\partial F}{\partial b_k} &= D\mathcal{P}(\mathbf{y}(\theta_j))\mathbf{I}_4 \sin(k\theta_j) - \mathbf{I}_4(\sin(k\theta_j + k\omega)). \end{aligned} \tag{15}$$

In Eq. (15) $D\mathcal{P}$ denotes the Jacobian of the flow corrected at Σ and $\mathbf{I}_4$ is the 4×4 identity matrix.

As pointed out by Castellà and Jorba (2000), there are problems in solving the linear system that appears in the Newton method due to the lack of unicity in the Fourier representation, given that the kernel of the matrix has dimension of at least one. Such issue is solved by adding an additional linear condition to the system of equations. Is suffices to impose that one of the components of $y(\theta)$ is zero when $\theta = 0$. This leads to a non-square linear system that has a unique solution and can be solved using, for example, Gaussian elimination with row pivoting.

2.3 Hyperbolic invariant manifolds of periodic orbits

Consider the Poincaré map $\mathcal{P}$ that has a fixed point $w \in \mathbb{R}^4$ with a pair of real eigenvalues, $\lambda > 1$ e $1/\lambda$, and a pair of complex conjugate eigenvalues, $a \pm ib$, with $|a \pm ib| = 1$. The unstable manifold W^u_w of w is tangent to the subspace spanned by the eigenvector $v \in \mathbb{R}^4$ associated to λ. Similarly, the stable manifold W^s_w of w is tangent to the subspace spanned by the eigenvector $v' \in \mathbb{R}^4$ associated to $1/\lambda$. An approximation of W^u_w and W^s_w is obtained through the numerical globalization of the manifolds obtained from the linearisation of the system of equations around w.

The computation of W^u_w is as follows. Let $\mathbf{y}(\zeta)$ be a parametric representation around the fixed point w, with $w = \mathbf{y}(0)$ and $\mathcal{P}(\mathbf{y}(\zeta)) \approx \mathbf{y}(\lambda\zeta)$. We define ζ_{max} such that the linear approximation is valid within a small tolerance ϵ, that is, $||w + \zeta v - \mathcal{P}(w + \frac{\zeta}{\lambda}v)|| < \epsilon$, and compute $\zeta_{min} = \zeta_{max}/\lambda$.

Now, let s be the desired length up to which the curve W^u_w is to be computed and let σ be an auxiliar parameter along W^u_w. Set a fixed step of arc-length Δs. If $\zeta_{min} \leqslant \sigma \leqslant \zeta_{max}$, then we set $\zeta = \sigma$ and integrate the equations of motion to get $\mathcal{P}^j(w + \zeta v)$, which gives the n-th point along W^u_w. Else, if $\sigma > \zeta_{max}$, we find ζ such that $\zeta_{min} \leqslant \zeta = \sigma/\lambda^k \leqslant \zeta_{max}$ and compute $\mathcal{P}^k(w + \zeta v)$, which gives n-th point along W^u_w.

To obtain the $(n+1)$-th point, we increment σ by a given $\Delta\sigma$. For every new point computed we check the distance d_n between the n-th point just computed and the previously computed point $n-1$. If $d_n < \Delta s$, we keep increasing σ and computing new points while $\sum_n d_n \leqslant s$. Else if $d_n > \Delta s$, we reduce $\Delta\sigma$, go back to the point $n-1$ and recompute the n-th point.

To compute W^s_w one must use the reverse mapping, that is, $\mathcal{P}^{-1}$ obtained from ϕ_{-t}. Alternatively, in the case of the systems with time reversal symmetry, we can take advantage of this feature to immediately obtain W^s_w from the data computed for W^u_w.

2.4 Hyperbolic invariant manifolds of two-dimensional tori

Let $f : \mathbb{R}^n \to \mathbb{R}^n$ be a endomorphism that defines a discrete dynamical system $\bar{y} = f(y)$ and suppose that f has a compact invariant set $\mathcal{T}$. Let $\mathbf{w} \in \mathcal{T}$ be a given point and let $(x, \mathbf{w}) \in \mathbb{R}^n \times \mathcal{T}$, we write the linearisation around $\mathcal{T}$ as

$$x_{t+1} = Df(\mathbf{w}_t)x_t,\ \ \mathbf{w}_{t+1} = f(\mathbf{w}_t). \tag{16}$$

Now, let us consider that $\mathcal{T}$ is a normally hyperbolic invariant torus with dimension r and that the function $\mathbf{w} = \mathbb{T}^r \to \mathcal{T} \in \mathbb{R}^n$ gives the inclusion of that torus. If the dynamics in $\mathcal{T}$ is conjugated to a rigid rotation given by $\theta = \theta + \omega$, with

ISSN 2176-5480

rotation vector $\omega \in \mathbb{R}^r$ such that $f(\mathbf{w}(\theta)) = \mathbf{w}(\theta + \omega)$, then Eq. (16) can be rewritten as the following quasi-periodic linear system

$$\bar{x} = \mathbf{A}(\theta)x, \quad \bar{\theta} = \theta + \omega, \tag{17}$$

where $\mathbf{A} \equiv Df(\mathbf{w}(\theta))$, with $\omega \cdot m \neq n, \forall m \in \mathbb{Z}^r \backslash \{0\}, n \in \mathbb{Z}$.

We assume that Eq. (16) is a reducible skew product and compute the eigenfunctions $\psi(\theta)$ of $\mathbf{A}(\theta)$, that are solutions to $\mathbf{A}(\theta)\psi(\theta) = \lambda T_\omega \psi(\theta)$, where T_ω is the operator $[T_\omega \psi](\theta) = \psi(\theta + \omega)$.

If $\mathbf{A}$ is a reducible matrix with a simple transversal Lyapunov spectrum such that all the Lyapunov multipliers are different and satisfy $\tau_1 > \tau_2 > \cdots > \tau_{n-r}$, $\tau_1 \neq 1$, $i = 1, \cdots, n-r$, we can employ a modified power method (see Wysham and Meiss (2006) for more details) to obtain the eigenfunctions associated to the dominant eigenvalues of the torus $\mathcal{T}$. Indeed, if the multipliers are distinct and $\mathbf{A}$ is a real matrix, there is a set of real eigenvalues $\lambda_i = \pm\tau_i$ and real eigenfunctions ψ_i of $\mathbf{A}(\theta)\psi(\theta) = \lambda T_\omega \psi(\theta)$. So, we start with an arbitrary initial vector $q^{(0)} = \sum_{i=1}^{n} \alpha_i \psi_i(\theta_0)$ that can be written as a linear combination of the eigenfunctions ψ_i at some θ_0, with $\alpha_1 \neq 0$. Then we define iterative sequences

$$u^{(k)} = \frac{q^{(k)}}{\parallel q^{(k)} \parallel} \quad \text{and} \quad q^{(k+1)} = \mathbf{A}(\theta_0 + k\omega)u^{(k)}, \tag{18}$$

such that $\prod_{j=0}^{k} \parallel q^{(j)} \parallel = \parallel \mathbf{A}^{(k)}(\theta_0)q^{(0)} \parallel$.

Let ψ_1 be the eigenfunction with dominant eigenvalue, then

$$u^{(k)} = \frac{\lambda_1^k}{\parallel \mathbf{A}(\theta_0)q^{(0)} \parallel}[\alpha_1\psi_1(\theta_0 + k\omega) + \mathcal{O}(\frac{\lambda_2}{\lambda_1})^k]. \tag{19}$$

Given that, by definition, $u^{(k)}$ is an unitary vector and ψ_1 is a continuous function, the coefficient of ψ_1 in Eq. (19) must be limited. Thus, if we define $s_k = \text{signal}(\lambda)^k$, we have

$$u^{(k)} \to s_k \frac{\psi_1(\theta_0 + k\omega)}{\parallel \psi_1(\theta_0 + k\omega) \parallel} \tag{20}$$

which is the eigenvector we look for, except for the choice of the signal, and the Lyapunov multiplier is obtained by

$$\tau_1 = \lim_{k\to\infty} (\prod_{j=0}^{k} \parallel q^j \parallel)^{1/k}. \tag{21}$$

Given that $\mathbf{A}$ is reducible, it has a dominant subspace. This implies that after a certain number of iterations the vector $u^{(k)}$ will align with the dominant eigenfunction. So we can select a subsequence k_j for which $\parallel k_j\omega \parallel_{\mathbb{Z}^r} \to 0$ in order to compute $\psi_1(\theta_0)$. The value of ψ_1 at every iteration is approximated using polynomial interpolation in $u^{(k_j)}$ through the points $\theta + k_j\omega$ along the curve. The iterative process stops when we obtain the desired accuracy in ψ_1.

Let the endomorphism f be the Poincaré map $\mathcal{P} : \mathbb{R}^4 \to \mathbb{R}^4$, then an invariant torus with $r = 2$ corresponds to a one-dimensional curve of $\mathcal{P}$. Once we compute the dominant eigenfunctions at several angles along the curve, we integrate initial conditions around the curve taken in an annular fundamental domain along the eigendirections and obtain a linear approximation of the unstable manifold of the torus. In the case of the SCR3BP, the stable manifold can be immediately obtained applying the symmetries of the system.

2.5 Continuation methods

Let $\mathbf{w}$ be a periodic solution of the Poincaré map $\mathcal{P} : \mathbb{R}^4 \to \mathbb{R}^4$ for a given value of a parameter ϵ such that $F(\mathbf{w}, \epsilon) = \mathcal{P}(\mathbf{w}, \epsilon) - \mathbf{w} = 0$.

In order to investigate how the solution behaves when ε changes by $\Delta\varepsilon$, we can write

$$\mathcal{P}(\mathbf{w} + \Delta\mathbf{w}, \varepsilon + \Delta\varepsilon) \simeq D_{\mathbf{w}}\mathcal{P}(\mathbf{w}, \varepsilon)\Delta\mathbf{w} + D_\varepsilon\mathcal{P}(\mathbf{w}, \varepsilon)\Delta\varepsilon, \tag{22}$$

where $D_{\mathbf{w}}\mathcal{P}$ is the Jacobian of the flow corrected at the Poincaré section with respect to the initial conditions and $D_\varepsilon\mathcal{P}$ is obtained by numerical integration of the variational equations

$$\dot{\mathbf{u}} = D_{\mathbf{u}}f \cdot \mathbf{u} + D_\varepsilon f, \tag{23}$$

with $\mathbf{u}(0) = 0$, where $\mathbf{u} \in \mathbb{R}^6$ is the Jacobian of the flow corrected at the section with respect to ε.

The most basic implementation of the continuation method (see Govaerts (1987) for more details) is to compute a few solutions changing ε, taking a suitable step $\Delta\varepsilon$, with the last computed solution as initial condition as an initial

ISSN 2176-5480

guess for the next one, and employing the Newton method to solve the linear system. Once some solutions are available, extrapolation (by means of Lagrange Polynomials, for example) with respect to ε is used to get the next guess for values of the variables. The step control must be performed based on the number of Newton iterates needed for the guess to converge to the solution. However, the continuation method fails at the points of return of the solution curve with respect to ε.

So, it is convenient to use the arc-length along the solution curve as the continuation parameter instead of the natural parameter ε. Then, the extrapolation is performed with respect to the arc-length and the solution moves past the points of return that could appear with respect to ε.

Another alternative is to employ the vector tangent to the curve of continued solutions to predict the next tentative solution: consider the $n \times (n+1)$ matrix $\mathbf{A} = DF$, where DF is the differential of F, and let $\mathbf{A}^T = P^T LU$ be the usual LU decomposition of a non-square matrix. Then,

$$L^T P y \;=\; [0 \;\cdots\; 0\; 1]^T = e_{m+1} \tag{24}$$

gives y, and the vector tangent to the solution curve is given by

$$\mathbf{v} = \sigma \frac{y}{\|y\|}, \tag{25}$$

where σ is $+1$, if $\det(P)\det(L)\det(U) > 0$, and -1 otherwise. Thus, a new guess for the modified Newton Method is given by $\mathbf{w}_{new} = \mathbf{w}_{old} + \epsilon \mathbf{A}$, where ϵ is a small parameter to be chosen.

3. NUMERICAL INVESTIGATION: APPLICATIONS AND RESULTS

In general, the numerical approach to investigate stability domains starts with the selection of sets of initial conditions in the phase space. Then these sets are integrated and an adequate algorithm is used to analyse if trajectories escape or remain confined for a given (long) span of time. This sorting process provides a visualization of the general shape of the practical stability region and allows the quantification of certain properties (see Simó (2006) and Simó and Vieiro (2007) for examples in different systems, particularly in the SCR3BP).

The next step is trying to identify which are the dynamical structures that play a role in defining the detected domains. To this end, we employ the procedures described in Section 2.

As an illustration of the employment of these techniques, in this paper we compute several invariant objects of the SCR3BP with $\mu_{SJ} = 9.538754 \times 10^{-4}$, which models the Sun-Jupiter system. We use FORTRAN for the implementation of the procedures, and integrate the system of ordinary differential equations by means of a Taylor method with variable order, using an ANSI C routine generated by *Taylor 1.4.4* (Jorba and Zou (2005)) and modified as needed.

We define the Poincaré map $\mathcal{P}_h : \Sigma_h \to \Sigma_h$, where $\Sigma_h = \{(x, y, z, \dot{x}, \dot{y}, \dot{z}) \in \mathbb{R}^6 | z = 0\} \cap \{H = h\}$, with $h = (\mu(1-\mu) - C)/2$, where C is known as the Jacobi constant and h is the corresponding energy.

We start showing examples of periodic orbits around L_3. In Fig. (1) we show the projection onto position space of periodic solutions in the center manifold of L_3, known as vertical and planar Lyapunov orbits, for three different values of C. Each vertical periodic orbit is a point of the map $\mathcal{P}_h$ corresponding to the h of the orbit. So, we find each of them as points of $\mathcal{P}_h$, as described in Section 2.1, and then integrate for a full period, that is, until the next intersection with the Poincaré plane, to get the one-dimensional curves shown in Fig. (1).

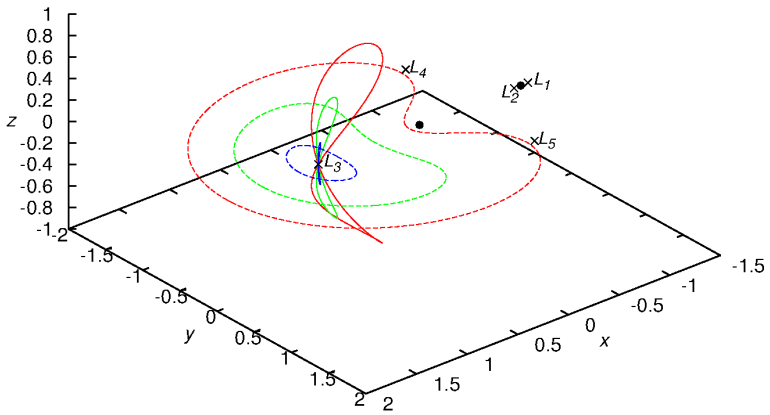

Figure 1. Vertical (solid lines) and planar (dashed lines) Lyapunov periodic orbits around L_3 for $C = 1.86791577$ (red), $C = 2.66050056$ (green), and $C = 2.96411566$ (blue). The primaries and the equilibrium points of the system are depicted with black points and xs, respectively.

ISSN 2176-5480

On the other hand, the planar Lyapunov orbits are completely contained in $\mathcal{P}_h$, therefore we must define alternative Poincaré sections in order to find them, using $x = constant$ or $y = constant$ instead of $z = 0$. Some possible choices are $x = x_{L_3} = 1.00039745$, where x_{L_3} denotes the position of L_3, or $y = 0$.

The vertical Lyapunov orbits, as well as the planar, form a uni-parametric family in the center manifold of L_3. Using C as the continuation parameter, in Fig. (2) we plot the two-dimensional surface formed by the vertical Lyapunov family from the beginning of the family at $C \lessapprox C_3 = 3.00019068$, with C_3 being the value of C at L_3, until $C \approx 8.25741135 \times 10^{-3}$. In that range of C, the orbits are unstable of center-saddle type in $\mathcal{P}_h$.

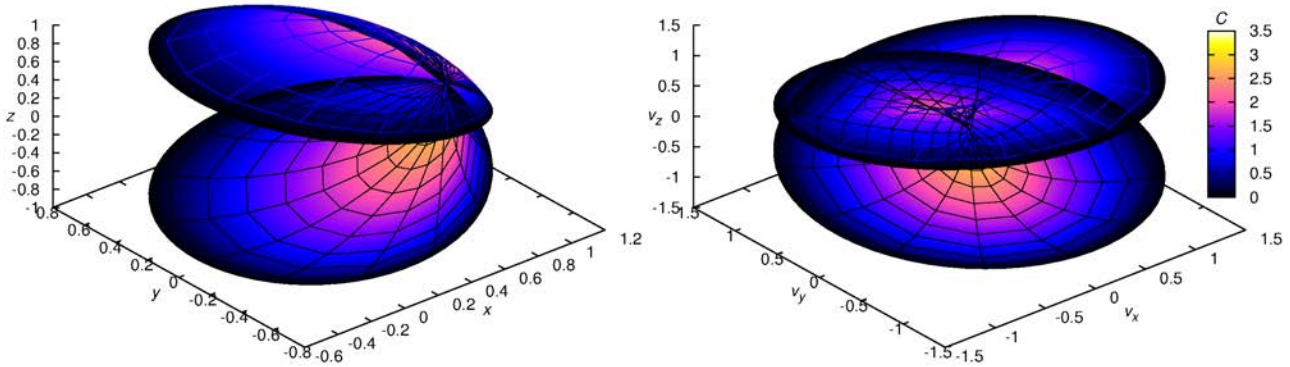

Figure 2. Projection onto position space (left) and onto velocity space (right) of the surface formed by the vertical Lyapunov family. The colours correspond to the values of C of the orbits.

Take $C = 2.96411566$ which gives $h = -2.96316269$. In $\mathcal{P}_h$, the Lyapunov orbit is a point and its hyperbolic manifolds are one-dimensional curves, as shown in Fig. (3). The projection onto the xy-plane (left frame of Fig. (3)) may misleadingly lead to conclusion that the stable and the unstable manifolds coincide. However, the projection onto $xy\dot{z}$-space (right frame of Fig. (3)) clearly shows that these manifolds have a small splitting.

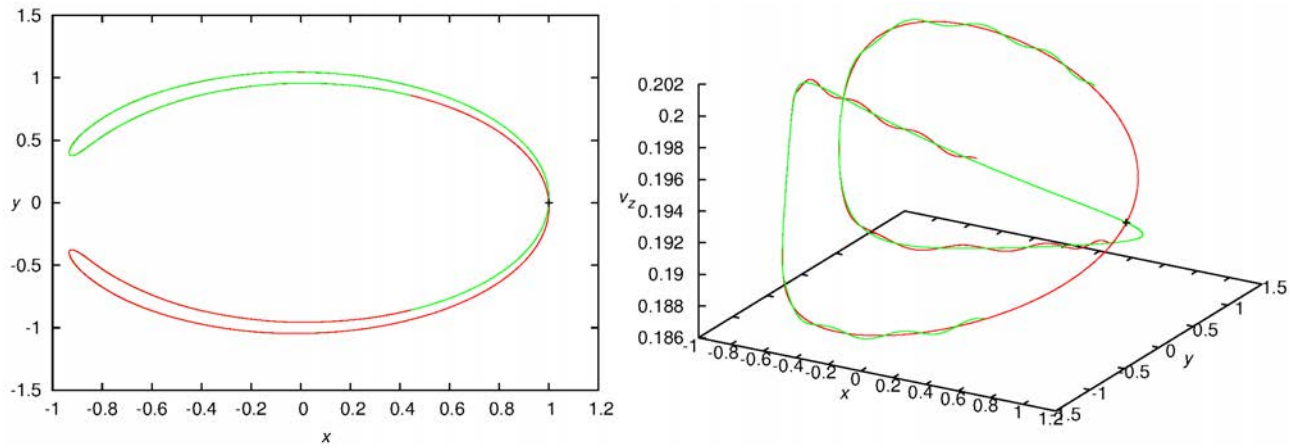

Figure 3. xy projection (left) and $xy\dot{z}$ projection of the Poincaré section ($z = 0, \dot{z} > 0$) of the stable (green) and the unstable (red) manifolds of the vertical Lyapunov orbit (black cross) around L_3 for $C = 2.96411566$.

The stable and the unstable manifolds of a periodic orbit are two-dimensional in the complete six-dimensional phase space. In fact, in the planar CR3BP (that can be viewed as a particular case of the SCR3BP) the center-saddle (planar) Lyapunov orbits in the center manifold of L_3 have hyperbolic manifolds that are locally homeomorphic to cylinders and act as separatrices in the energy level. In that case, the three-dimensional surface formed by these hyperbolic manifolds are codimension-1 in the phase space and account for the effective confinement of trajectories in a large vicinity of L_5 (Gómez *et al.* (2001b)). On the other hand, in the SCR3BP, it is expected that higher dimensional invariant structures in the center manifold of L_3 replace the periodic orbits in playing a role in the definition of the practical stability boundaries around L_5, at least for trajectories with small vertical amplitude. Indeed, Simó *et al.* (2013a) observed that at least two Cantorian families of two-dimensional hyperbolic tori are related to the practical stability boundaries for small values of the mass parameter.

Figure (4) shows the Poincaré section of several two-dimensional hyperbolic tori of the Cantorian family that connects the vertical and the planar Lyapunov orbits in the center manifold of L_3 for $C = 2.96411566$. In $\mathcal{P}_h$ these tori correspond to one-dimensional curves with different rotation number ρ which are found for fixed C, through the method described in Section 2.2, starting from the vertical periodic orbit and employing continuation, with the rotation number as the

ISSN 2176-5480

continuation parameter, to reach the planar periodic orbit.

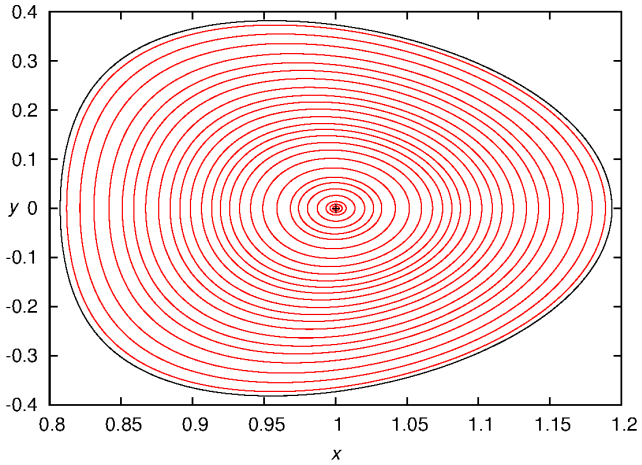

Figure 4. The red curves are the xy-projection of the Poincaré section of several two-dimensional tori with $C = 2.96411566$. The black cross is the projection of the Poincaré section of the vertical Lyapunov and the black curve is the projection of the planar Lyapunov.

The two-dimensional tori in the center manifold of L_3 form a Cantorian bi-parametric family in the phase space. The vertical amplitude of these invariant solutions is maximal near the vertical Lyapunov orbit and decreases until they reach the planar Lyapunov orbit. Figure (5) shows the projection onto position space of the full trajectories of two tori with different rotation numbers. The curves with $\rho = 4.15672285 \times 10^{-4}$ and $\rho = 4.02411492 \times 10^{-4}$ were represented with 18 and 20 Fourier modes, respectively. Then, points along the curve were selected as initial conditions and integrated to get the quasi-periodic trajectories shown in Fig. (5).

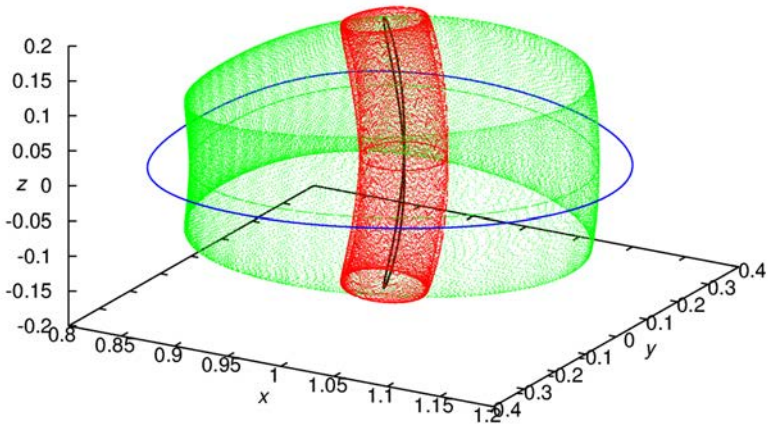

Figure 5. Projection onto position space of the trajectories of two tori with $\rho = 4.15672285 \times 10^{-4}$ (red) and $\rho = 4.02411492 \times 10^{-4}$ (green) for $C = 2.96411566$. The vertical and the planar Lyapunov orbits are shown in black and in blue, respectively.

The hyperbolic invariant manifolds of each torus of the family are three-dimensional objects in the six-dimensional phase space. In Fig. (6) we plot the two-dimensional surface obtained by considering a Poincaré section of the manifolds of the torus with $\rho = 4.13260566243 \times 10^{-4}$. To account for the third dimension, we use τ, a normalized parameter related to the number of initial conditions taken along the eigendirections within an annular fundamental domain to generate orbits on the manifolds. Negative values of τ correspond to the stable branches of the hyperbolic manifold, while positive values of τ correspond to the unstable branches of the hyperbolic manifold.

The implemented algorithm, based on the method described in Section 2.4, stops the computation of each orbit along the upper (lower) branch of the unstable manifold just after the trajectories cross the line that connects L_5 (L_4) to the larger primary. For the example in Fig. (6), the average computation time of each unstable branch is of the order of 10^3 seconds using an Intel ® Core (TM) i7-2640M, 2,8GHz with 4 processors. Typically the running time decreases with C and increases as ρ decreases. The stable manifolds are immediately obtained by symmetry from the computed unstable manifolds.

Finally, let γ_0 be the invariant curve that represents a two-dimensional torus T^2 in $\mathcal{P}_h$. We define several curves γ_i,

ISSN 2176-5480

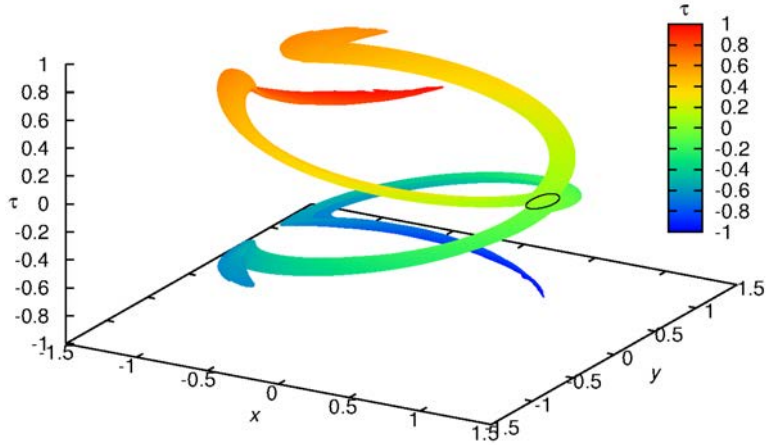

Figure 6. Stable and unstable manifolds of the two-dimensional hyperbolic torus with $C = 2.96411566$ and $\rho = 4.13260566243 \times 10^{-4}$, depicted as a black curve at $\tau = 0$. Negative and positive values of τ correspond, respectively, to the stable and the unstable branches of the hyperbolic manifold.

$i = 1, ..., k$, near γ_0 and along its unstable eigendirection such that the distance from γ_i to γ_0 is r_i, where r_i is a constant number for each γ_i. Then, we select points in γ_i as initial conditions and integrate the trajectories for a given number of Poincaré iterates to get orbits that are an approximation of the unstable manifold of T^2. Then we plot the n-th iteration of all initial conditions of a single γ_i together. This is equivalent to computing a stroboscopic map with period equal to one Poincaré iteration of the orbit. Figure 7 shows such a map for some selected pairs of (i, n). We can see how the unstable manifold departs from T^2 and deforms as n increases.

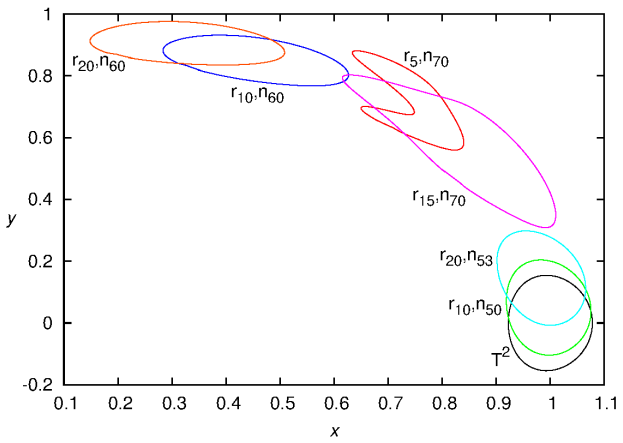

Figure 7. Unstable manifold of the two-dimensional invariant torus with $C = 2.96411566$ and $\rho = 4.13260566243 \times 10^{-4}$. T^2 stands for the curve γ_0 and the curves labeled with r_i, n_n correspond to the n-th iteration of the initial conditions taken on γ_i.

4. FINAL REMARKS

We described methods to compute invariant objects and applied them to the study of the SCR3BP, using the mass parameter corresponding to the Sun-Jupiter system. Specifically, we computed vertical and planar Lyapunov orbits of center-center-saddle type around L_3 and showed that the stable and unstable invariant manifolds of the vertical Lyapunov orbits split. Additionally, we computed two-dimensional hyperbolic tori in the center manifold of L_3 and obtained the stable and unstable manifolds of a torus for a pair of Jacobi constant and rotation number.

Once the procedures and their implementations are validated they can be used to perform a systematic investigation of the objects that determine effective stability boundaries of the Sun-Jupiter system. For this, one has to perform correspondence checks between numerically constructed invariant structures and approximated solutions obtained from the analysis of capture-escape transitions.

ISSN 2176-5480

5. ACKNOWLEDGEMENTS

This contribution is part of the outcome of joint work with Prof. Dr. Carles Simó to whom the authors are greatly indebted. P.A. Sousa-Silva thanks CNPq (Brazil) for the grant PDE-201932/2010-5. M.O. Terra thanks FAPESP (Brazil) for the grants 2010/18692-8 and 2012/21023-6.

6. REFERENCES

Benet, L., 2001. "Occurence of planetary rings with shepherds". *Celestial Mechanics and Dynamical Astronomy*, Vol. 81, pp. 123–128.

Castellà, E. and Jorba, A., 2000. "On the vertical families of two-dimensional tori near the triangular points of the Bicirbular Problem". *Celestial Mechanics and Dynamical Astronomy*, Vol. 76, pp. 35–54.

Giorgilli, A., Delshams, A., Fontich, E., Galgani, L. and Simó, C., 1989. "Effective stability for a Hamiltonian system near an elliptic equilibrium point, with an application to the Restricted Three-Body Problem". *Journal of Differential Equations*, Vol. 77, pp. 167–370.

Gómez, G., Jorba, A., Simó, C. and Masdemont, J., 2001a. *Dynamics and Mission Design Near Libration Points, Volume III: Advanced Methods for Collinear Points*. World Scientific.

Gómez, G., Jorba, A., Simó, C. and Masdemont, J., 2001b. *Dynamics and Mission Design Near Libration Points, Volume IV: Advanced Methods for Triangular Points*. World Scientific.

Gómez, G., Llibre, J., Martínez, R. and Simó, C., 2001c. *Dynamics and Mission Design Near Libration Points, Volume I: Fundamentals: The Case of Collinear Libration Points*. World Scientific.

Gómez, G., Simó, C., Llibre, J. and Martínez, R., 2001d. *Dynamics and Mission Design Near Libration Points, Volume II: Fundamentals: The Case of Triangular Libration Points*. World Scientific.

Govaerts, W., 1987. *Numerical Methods for Bifurcations of Dynamical Equilibria*. SIAM.

Jorba, A. and Zou, M., 2005. "A software package for the numerical integration of ODEs by means of high-order Taylor methods". *Experimental Mathematics*, Vol. 14, pp. 99–117.

Koon, W., Lo, M., Marsden, J. and Ross, S., 2006. *Dynamical Systems, The Three-Body Problem, And Space Mission Design*. Springer-Verlag.

Markeev, A., 1972. "Stability of the triangular Lagrangian solutions of the Restricted Three-Body Problem in the three-dimensional circular case". *Soviet Astronomy*, Vol. 15, pp. 682–686.

Marsden, J. and Ross, S., 2005. "New methods in celestial mechanics and mission design". *Bulletin (New Series) of the American Mathematical Society*, Vol. 43, pp. 43–73.

MPC, 2013. "Website of the Minor Planet Center - Smithsonian Astrophysical Observatory". Last access: 22 May 2013 <http://www.minorplanetcenter.net>.

NASA, 2013. "Website of the Near-Earth Object Program". Last access: 22 May 2013 <http://neo.jpl.nasa.gov>.

Robutel, P. and Souchay, J., 2010. *Dynamics of Small Solar System Bodies and Exoplanets*, Springer, chapter An introduction to the dynamics of Trojan asteroids. Number 790 in Lecture Notes in Physics.

Simó, C., 1990. *Modern Methods in Celestial Mechanics*, Editions Frontières, chapter On the Analytical and Numerical Approximation of Invariant Manifolds, pp. 285–329.

Simó, C., 1998. "Effective computations in Celestial Mechanics and Astrodynamics". In V. Rumyantsev and A. Karapetyan, eds., *Modern Methods of Analytical Mechanics and their Applications*. Springer, Vol. 387 of *CISM Courses and Lectures*, pp. 55–102.

Simó, C., 2006. "Boundaries of stability". <http://maia.ub.es/dsg/2006/> number 2.

Simó, C., Sousa Silva, P. and Terra, M., 2012. "Domains of practical stability near L4,5 in the 3D Restricted Three-Body Problem". <http://www.maia.ub.edu/dsg/2012/> number 8.

Simó, C., Sousa-Silva, P. and Terra, M., 2013a. "Domains of practical stability and hyperbolic structures near the triangular Lagrangian points in the 3D R3BP". To be submitted.

Simó, C., Sousa Silva, P. and Terra, M., 2013b. "Practical stability domains near L4,5 in the Restricted Three-Body Problem: some preliminary facts". In S. Ibáñez, J. Pérez del Río, A. Pumariño and J. Rodríguez, eds., *Progress and Challenges in Dynamical Systems*. Springer Proceedings in Mathematics and Statistics. To be published.

Simó, C. and Vieiro, A., 2007. "Towards a global study of Area Preserving Maps: Examples, models and applications". <http://www.maia.ub.es/dsg/2007/> number 13.

Szebehely, V., 1967. *Theory of Orbits*. Academic Press.

Wiggins, S., 2003. *Introduction to applied nonlinear dynamical systems and chaos*, Vol. 2 of *Texts in Applied Mathematics*. Springer, 2nd edition.

Wysham, D. and Meiss, J., 2006. "Iterative techniques for computing the linearized manifolds of quasiperiodic tori". *Chaos*, Vol. 16, No. 023129.

ISSN 2176-5480

7. RESPONSIBILITY NOTICE

The authors are the only responsible for the printed material included in this paper.